SLAC-PUB-15021

Femtosecond single-shot imaging of nanoscale ferromagnetic order in Co/Pd multilayers using resonant x-ray holography

Tianhan Wang,[1,2,*] Diling Zhu,[3,4] Benny Wu,[2,4] Catherine Graves,[2,4] Stefan Schaffert,[5] Torbjörn Rander,[5] Leonard Müller,[6] Boris Vodungbo,[7] Cédric Baumier,[8] David P. Bernstein,[2,4] Björn Bräuer,[2] Vincent Cros,[9] Sanne de Jong,[3] Renaud Delaunay,[8] Andreas Fognini,[10] Roopali Kukreja,[1,2] Sooheyong Lee,[3] Victor Lopéz-Flores,[11] Jyoti Mohanty,[5] Bastian Pfau,[12,5] Horia Popescu,[13] Maurizio Sacchi,[13] Anna B. Sardinha,[7,14] Fausto Sirotti,[13] Philippe Zeitoun,[7] Marc Messerschmidt,[3] Joshua J. Turner,[3] William F. Schlotter,[3] Olav Hellwig,[15] Richard Mattana,[9] Nicolas Jaouen,[13] Franck Fortuna,[16] Yves Acremann,[10] Christian Gutt,[6] Hermann A. Dürr,[2] Eric Beaurepaire,[11] Christine Boeglin,[11] Stefan Eisebitt,[12,5] Gerhard Grübel,[6] Jan Lüning,[8] Joachim Stöhr,[2,3] and Andreas O. Scherz[2,†]

[1]*Department of Materials Science and Engineering, Stanford University, Stanford, California 94035, USA*

[2]*Stanford Institute for Materials & Energy Science (SIMES), SLAC National Accelerator Laboratory, 2575 Sand Hill Road, Menlo Park, California, 94025, USA*

[3]*Linac Coherent Light Source, SLAC National Accelerator Laboratory, 2575 Sand Hill Road, Menlo Park, California 94025, USA*

[4]*Department of Applied Physics, Stanford University, Stanford, California 94035, USA*

[5]*Institut für Optik und Atomare Physik, Technische Universität Berlin, Straße des 17. Juni 135, 10623 Berlin, Germany*

[6]*Deutsches Elektronen-Synchrotron (DESY), Notkestr. 85, D-22607 Hamburg, Germany*

[7]*Laboratoire d'Optique Appliquée, ENSTA ParisTech - CNRS UMR 7639 - École Polytechnique, Chemin de la Hunière, 91761 Palaiseau, France*

[8]*Laboratoire de Chimie Physique - Matière et Rayonnement, Université Pierre et Marie Curie - CNRS UMR 7614, 11 rue Pierre et Marie Curie, 75005 Paris, France*

Division of Materials Sciences and Engineering, under contract DE-AC02-76SF00515 and BES.

[9] *Unité Mixte de Physique CNRS/Thales and Univerité Paris Sud 11, 1 ave A. Fresnel, 91767 Palaiseau, France*

[10] *Laboratorium f. Festkörperphysik, ETH Zürich, 8093 Zürich, Switzerland*

[11] *Institut de Physique et de Chimie des Matériaux de Strasbourg, UMR7504, CNRS et Universitié de Strasbourg, 23 rue du Loess, 67034 Strasbourg, France*

[12] *Helmholtz-Zentrum Berlin für Materialien und Energie GmbH, Hahn-Meitner-Platz 1, 14109 Berlin, Germany*

[13] *Synchrotron SOLEIL, L'Orme des Merisiers, Saint-Aubin, BP 48, 91192 Gif-sur-Yvette Cedex, France*

[14] *Grupo de Lasers e Plasmas - Instituto de Plasmas e Fusão Nuclear, Instituto Superior Técnico, Av. Rovisco Pais, 1049-001 Lisbon, Portugal*

[15] *San Jose Research Center, Hitachi Global Storage Technologies, 3403 Yerba Buena Road, San Jose, California 95135, USA*

[16] *Centre de Spectrométrie Nucléaire et de Spectrométrie de Masse, CNRS/IN2P3, Université Paris-Sud, UMR 8609, 91405 Orsay, France*

(Dated: May 15, 2012)

Abstract

We present the first single-shot images of ferromagnetic, nanoscale spin order taken with femtosecond x-ray pulses. X-ray-induced electron and spin dynamics can be outrun with pulses shorter than 80 fs in the investigated fluence regime, and no permanent aftereffects in the samples are observed below a fluence of 25 mJ/cm^2. Employing resonant spatially-muliplexed x-ray holography results in a low imaging threshold of 5 mJ/cm^2. Our results open new ways to combine ultrafast laser spectroscopy with sequential snapshot imaging on a single sample, generating a movie of excited state dynamics.

PACS numbers: 42.40.Kw, 42.55.Vc, 78.70.Ck, 78.47.J-

Keywords: X-ray Holography, X-ray Laser, Single-Shot Imaging

The advent of x-ray free electron lasers (XFELs) has opened the door for imaging atomic, electronic and magnetic structures of matter on their intrinsic atomic lengthscales and femtosecond timescales. The key question in single-shot x-ray imaging is the validity of the "probe-before-damage" concept based on capturing an image before manifestation of radiation damage [1]. This concept has been shown to hold for macroscopic sample destruction [2–4] and even for its atomic modification [5, 6]. Here we address whether and when this carries over to the more quickly responding and fragile valence electronic and magnetic structures.

A large variety of systems in soft, hard and biological matter contain nanoscale heterogeneities governed by underlying electronic structures and competing local interactions. This mesoscopic organization mediates atomic and macroscopic dimensions and determines functionality and macroscopic properties. The understanding of such ordering and relevant dynamics is of fundamental interest [7] and important for tailoring and utilizing their properties in nanotechnology. However, experimental studies of these materials on both the relevant length and timescales have been limited. XFELs such as the Linac Coherent Light Source (LCLS) [8] promise to fill this gap by giving access to nanoscale phenomena at timescales pertinent to the motion of atoms, charges and spins. Although coherent x-ray scattering can yield spatial frequency information [9], imaging is necessary to recover the complete real-space structure. Consequently, single-shot imaging has become an essential tool in the study and characterization of transient states during both stochastic and deterministic ultrafast, nanoscale dynamics. In particular, single-shot imaging is vital in the study of speed limits in technological processes [10, 11] since it can elucidate the involved transient states where such temporal processes cease to be repeatable [12].

While the attainable resolution in single-shot coherent diffractive imaging is typically determined by photon flux, the onset of radiation damage will render imaged states meaningless. It has been proposed that with short femtosecond pulses, one can outrun the damage processes and obtain atomic lengthscale structural information before atomic motion sets in [1]. This concept was recently demonstrated by recovering the structure of protein nanocrystals with 70 fs and shorter x-ray pulses [5]. However, even before internal Coulomb forces start moving the atoms apart, the faster processes of photoabsorption and photoionization with subsequent screening, Auger decay and secondary electron cascades set in within a few femtoseconds, and can dramatically change the electronic response [13, 14]. Any x-ray

induced electronic damage will therefore dictate the time frame in which the image of the underlying, nanoscale valence electronic structure must be captured.

Here we demonstrate single-shot imaging of the spin-resolved electronic structure of the 3d valence shell in a nanoscale-ordered magnetic film. For 80 fs pulses, no manifestation of damage is observed during the pulse. For the longer 360 fs pulses, demagnetization due to the thermalization of electrons and subsequent equilibration with the spin reservoir and the lattice is observed during the pulse. Using resonant x-ray spectro-holography [15] combined with sample spatial multiplexing [16], we achieve an imaging fluence threshold of $5\,\mathrm{mJ/cm^2}$ which corresponds to 4×10^5 photons/μm^2. This fluence is smaller by a remarkable 5 orders of magnitude than that used in destructive x-ray crystallography experiments at hard x-ray wavelengths [5, 6]. The damage threshold is $25\,\mathrm{mJ/cm^2}$, above which the x-ray pulse induces irreversible changes after the pulse through heating on picosecond timescales. Non-destructive and repeatable single-shot imaging is possible in the regime between these two thresholds. Future ultrafast studies of the spin system can therefore combine pump-probe techniques using variable time delays with a sequence of snapshots captured on a single sample, thereby generating a femtosecond "movie" of excited state dynamics.

We record individual diffraction patterns from a magnetic sample with an integrated holographic mask (Fig. 1), referred to as single-shot x-ray spectro-holography. For the experiments we chose sputter-deposited $\mathrm{Ta_{1.5nm}Pd_{3nm}(Co_{0.5nm}/Pd_{0.7nm})_{40}Pd_{2nm}}$ multilayers on $\mathrm{Si_3N_4}$ membranes which have been studied extensively as a candidate system for perpendicular recording media [17, 18]. When demagnetized in an external perpendicular AC field, the samples show a metastable configuration of ferromagnetic labyrinth-like nanoscale stripe domains of 100 nm in width, which sensitively depend on both external and internal parameters [17]. An 800 nm thick Au film, opaque to soft x-rays, is sputtered on the back side of the membrane. A focused ion beam is then used to mill a 1.45 μm field-of-view (FOV) aperture through the Au with five or fifteen 100 nm diameter reference holes milled through the entire sample, forming the holography mask.

By tuning the LCLS x-ray pulses to the Co L_3 absorption resonance, the spin orientation in the ferromagnetic domains is resolved through the x-ray magnetic circular dichroism (XMCD) effect [19]. X-ray pulses of up to 1.87 mJ are sent through a grating monochromator to select the photon energy (778.8 eV) with an energy resolution of 0.5 eV [20]. As LCLS only produces linearly polarized x-rays, a 40nm, in-plane-magnetized Co magnetic thin film

polarizer is used to generate circular polarization [21]. The unfocused monochromatic beam is therefore sent through the polarizer at 60 degrees to the incident x-rays, producing up to 10^9 photons per pulse with 58% circular polarization. The large beam spot size at the polarizer results in a low energy density ($<1\,\mathrm{mJ/cm^2}$) and the magnetization of the polarizer film remains fixed by a permanent magnet. A spot size of 10 by $30\,\mu$m is achieved at the sample by focusing the beam with bendable Kirkpatrick-Baez mirrors [22]. Finally, the x-ray holograms are recorded with a back-illuminated in-vacuum charge-coupled-device (CCD) detector with 2048x2048 pixels of 13.5x13.5 $\mu\mathrm{m}^2$ that is mounted on a translational stage to adjust the sample-detector distance. A CCD numerical aperture of 0.0282 is chosen at a 490 mm distance, giving a maximum momentum transfer of $0.111\,\mathrm{nm}^{-1}$ for 1.59 nm wavelength (Co L_3 edge). The holographic mask contains multiple reference holes, each of which produces a snapshot of the sample, cf. Fig. 1a. As the phase information is encoded by the sample-reference interference, a single Fourier inversion of the diffraction pattern recovers the real space image [15]. Initial domain patterns are reconstructed from many low-fluence x-ray pulses, see Fig. 1b-c. Subsequently, a series of single-shot images are collected with 80 and 360 fs x-ray pulses at higher fluences.

Fig. 2a shows a single-shot diffraction pattern from an 80 fs pulse. With circularly polarized x-rays, the pattern forms due to charge-magnetic interference (CMI) of the sample and reference waves [23], where the resonant charge and magnetic scattering contrasts are proportional to the vacancies and the spin-splitting of the 3d valence states, respectively. In Fig. 2b-c, the strategic placement of the references produces well-separated images of the spin-resolved electronic structure in the autocorrelation after the Fourier inversion. Each reference generates an independent reconstruction - a pair of radially opposite complex-conjugates in the autocorrelation. Due to uneven beam profile and beam position jitter, not all the references may be illuminated equally during a pulse, resulting in different image qualities. The reconstructions without sufficient signal-to-noise-ratio (SNR) are then discarded during averaging. The summation over all independent reconstructions significantly improves the image quality, enhancing the SNR by up to a factor of 4 (for 15 references) [16]. The combination of resonantly-enhanced scattering with spatially-multiplexed x-ray holography operates at photon fluences 2 orders of magnitude less than phase retrieval methods, mitigating possible damage during and after the XFEL pulse. We determined an imaging threshold of $5\,\mathrm{mJ/cm^2}$ for our sample system [24]. Due to the stochastic intensity jitter at

LCLS, reconstructions were achieved for approximately half of the x-ray pulses used.

To capture the true prepared states of interest, x-ray induced modifications should not appear during the probe pulse. At a fluence of $20\,\mathrm{mJ/cm^2}$, approximately 1 in 1000 Co atoms absorbs a photon. The core holes in the L-shell decay via the dominant Auger channel (99%) within a few femtoseconds. Model calculations based on ref. [25] show that the electronic damage sets in when Auger electrons generate a cascade of secondary electrons in the sample with a typical collision rate of 1/fs, transferring 3d electrons into the continuum. Within several tens of femtoseconds the energy, 0.8 eV/atom on average, is effectively distributed over all atomic sites producing a hot electron gas in the valence band that thermalizes in about 100 fs [26]. Subsequently, energy and angular momentum is transferred on characteristic time-scales to the spin (150-300 fs) and phonon ($\geq$0.5 ps) systems, leading to ultrafast demagnetization and heating of the lattice [27–29].

We studied damage during the pulse by analyzing the CMI intensity as a function of fluence and pulse duration shown in Fig. 3. To determine the relative CMI intensities for single-shots at different fluences, we compare the CMI contrast from the reconstructions. The single-shot diffraction patterns are normalized based on the photon intensity relative to the low fluence reconstruction of the starting domain state. Data after intense x-ray pulses shots are discarded when the sample was significantly altered as described further below. For 80 fs pulses, the CMI intensity remains proportional to the incident fluence up to $28\,\mathrm{mJ/cm^2}$, suggesting that the sample state does not change significantly during the pulse. It should be noted that the reported pulse durations refer to electron bunch length measurements and may be considerably shorter, as suggested by the electronic response of atoms to intense x-rays beams [13]. For pulses nominally 4 times longer, we find a decrease in the CMI intensity at higher intensities, indicative of x-ray-induced demagnetization triggered by secondary-electron cascades during the pulse. As a result, the time frame must be set to $\leq$80 fs for probing the prepared state of interest in this fluence regime. This decrease can be explained in terms of the known laser-induced ultrafast demagnetization at optical wavelengths [26–29] when the absorption of x-rays deposits about the same amount of energy over the sample volume as compared to optical pumping. A simple model is used to calculate the ultrafast demagnetization process (Fig. 3, red line), during which the sample magnetization decreases linearly with increasing fluence until the sample is completely demagnetized at a threshold fluence [27]. The characteristic time scale of this ultrafast process is set to 280 fs which

corresponds to reported values [29]. The 360 fs pulses were then divided into 10 fs slices and propagated through the sample and the resulting CMI intensity was integrated over the pulse.

Ultrafast pump-probe spectroscopy by sequential imaging at destructive fluences will be limited to the accuracy of cloning solid state targets with confined object regions and reproducible positioning in the XFEL beam. Therefore, to assemble a movie of ultrafast processes, it is desirable that a single specimen can withstand the aftereffects caused by picosecond-scale thermal heating and can be reset to the initial state for the next shot. The feasibility of nondestructive, sequential single-shot imaging is demonstrated in Fig. 4a for 360 fs pulses (similar data, not shown here, are also obtained for 80 fs pulses). Back-to-back snapshots produce highly correlated ($\geq 75\%$) images, cf. Fig. 4b-c and d-e, with only minor lateral fluctuations along the domain borders near the 25 mJ/cm^2 boundary. At the Co L_3 absorption edge, the Co/Pd multilayers absorb 83% of the photons with 70% of the total energy deposited in Co. At 25 mJ/cm^2 x-ray fluence, the average temperature in the sample would reach 1100 K, not accounting for heat transfer. Beyond 25 mJ/cm^2, temperatures above the Curie temperature of 750 K [30] have been reached and the demagnetized sample forms a new domain pattern upon cooling. In Fig. 4d-e, the altered nanoscale periodicity suggests irreversible thermal damage caused by interstitial diffusion across Co/Pd interfaces and subsequent anisotropy softening [9]. The key to nondestructive sequential imaging is to utilize the regime between the minimum imaging and the thermal damage thresholds.

In summary, the results presented here demonstrate the feasibility of highly efficient single-shot imaging of the spin-resolved electronic structure. The strong interaction of intense x-ray beams with the electronic system causes damage to the spin structure that can be outrun with pulses $\leq$80 fs. Enhancements in resolution can be achieved at higher fluences with smaller x-ray focuses at the expense of sample destruction, and by using holography techniques such as uniformly redundant arrays [4] and differential holographic imaging [31]. The demonstrated feasibility of nondestructive sequential single-shot imaging provides a very attractive tool for the time-resolved study of nanoscale femtosecond dynamics. Future upgrades to LCLS for full polarization control of the x-ray beam will render the polarizer unnecessary, providing a two-order magnitude increase in photon flux. Proposed seeded XFEL sources will further enhance flux and reduce intensity jitters. Such improvements will significantly increase the photon-limited resolution for destructive imaging and enable

resonant phase imaging at energies where the radiation dose is 10 times lower compared with the peak-absorption [32]. The considerable shift of damage thresholds will further extend the current spatial resolution of 50-80 nm for nondestructive sequential single-shot imaging. Our results open new ways to study the nanoscale charge and spin dynamics in materials by ultrafast x-ray laser spectroscopy.

ACKNOWLEDGEMENTS

The experiments were carried out at the SXR beamline at LCLS and the beamline 13.3 at SSRL using the Resonant Coherent Imaging (RCI) endstation, both national user facilities operated by Stanford University on behalf of the U.S. Department of Energy, Office of Basic Energy Sciences. The SXR instrument is funded by a consortium whose membership includes the LCLS, Stanford University through SIMES, Lawrence Berkeley National Laboratory (LBNL), University of Hamburg through the BMBF priority program FSP 301, and the Center for Free Electron Laser Science (CFEL). We would like to gratefully acknowledge support from the following: U.S. Department of Energy, Office of Basic Energy Sciences, Division of Materials Sciences and Engineering, under contract DE-AC02-76SF00515; German Federal Ministry for Education and Research under contract BMBF-05K10KTB; ETH Zürich; CNRS via the PEPS SASELEX (Soutien aux activités scientifiques françaises autour des lasers à électrons libres émettant des rayons X) and FCT - Portuguese Foundation for Science and Technology.

* wangth@stanford.edu; corresponding author. Phone: +1 650 926 2535 Fax: +1 650 926 4100

† ascherz@stanford.edu; corresponding author. Phone: +1 650 926 3829 Fax: +1 650 926 4100

[1] R. Neutze *et al.*, Nature **406**, 752 (2000).

[2] H. N. Chapman *et al.*, Nature Phys. **2**, 839 (2006).

[3] A. Barty *et al.*, Nature Photon. **2**, 415 (2008).

[4] S. Marchesini *et al.*, Nature Photon. **2**, 560 (2008).

[5] H. N. Chapman *et al.*, Nature **470**, 73 (2011).

[6] M. M. Seibert *et al.*, Nature **470**, 78, (2011).

[7] R. B. Laughlin, D. Pines, J. Schmalian, B. P. Stojković, and P. Wolynes, Proc. Nat. Acad. Sci. USA **97**, 32 (2000).

[8] P. Emma *et al.*, Nature Photon. **4**, 641 (2010).

[9] C. Gutt *et al.*, Phys. Rev. B **81**, 100401 (2010).

[10] I. Tudosa *et al.*, Nature **428**, 831 (2004).

[11] C. Stanciu *et al.*, Phys. Rev. Lett **99**, 047601 (2007).

[12] B. Wu *et al.*, Appl. Phys. Lett. **99**, 252505 (2011).

[13] L. Young *et al.*, Nature **466**, 56 (2010).

[14] S. P. Hau-Riege, R. A. London, and A. Szoke, Phys. Rev. E **69**, 051906 (2004).

[15] S. Eisebitt *et al.*, Nature **432**, 885 (2004).

[16] W. F. Schlotter *et al.*, Appl. Phys. Lett. **89**, 163112 (2006).

[17] O. Hellwig, G. P. Denbeaux, J. B. Kortright, and E. E. Fullerton, Physica B **336**, 136 (2003).

[18] O. Hellwig, A. Berger, J. B. Kortright, and E. E. Fullerton, J. Magn. Magn. Mater. **319**, 13 (2007).

[19] J. Stöhr *et al.*, Science **259**, 658 (1993).

[20] P. Heimann *et al.*, Rev. Sci. Instrum. **82**, 093104 (2011).

[21] B. Pfau *et al.*, Opt. Express **18**, 13608 (2010).

[22] J. Chalupsky *et al.*, Nucl. Instrum. Meth. A **631**, 130 (2011).

[23] S. Eisebitt *et al.*, Phys. Rev. B **68**, 104419 (2003).

[24] With binary magnetic domains, we express the CMI contrast as the standard deviation of the pixels within the circular FOV aperture. Correspondingly, shot noise determines the spread in

the background outside of the FOV. The imaging threshold is then defined as when the CMI contrast is more than twice the standard deviation of background noise (SNR >2).

[25] R. Knorren, K. H. Bennemann, R. Burgermeister, and M. Aeschlimann, Phys. Rev. B **61**, 9427 (2000).

[26] H.-S. Rhie, H. A. Dürr, and W. Eberhardt, Phys. Rev. Lett. **90**, 247201 (2003).

[27] B. Koopmans *et al.*, Nature Mater. **9**, 259 (2010).

[28] C. Stamm *et al.*, Nature Mater. **6**, 740 (2007).

[29] C. Boeglin *et al.*, Nature **465**, 485 (2010).

[30] T. Hauet *et al.*, Phys. Rev. B **77**, 184421 (2008).

[31] D. Zhu *et al.*, Phys. Rev. Lett. **105**, 043901 (2010).

[32] A. Scherz *et al.*, Phys. Rev. B **76**, 214410 (2007).

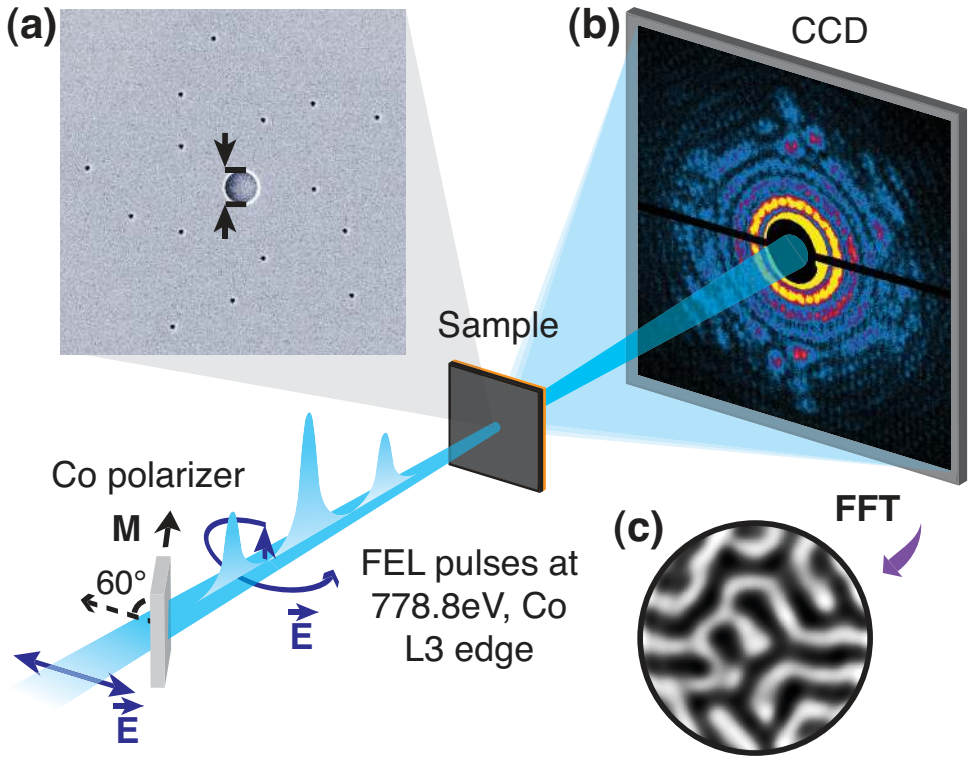

FIG. 1. The experimental setup. **a**, Scanning electron microscopy image of a 15-reference gold holography mask, showing the aperture and the references. Samples with 5 references contain the inner ring of references only. The sample aperture diameter is 1.45 μm (two markers), and the references are 100 nm in diameter. **b**, A CCD camera located 490 mm downstream (numerical aperture of 0.028) records the spectro-hologram in the far-field. A tungsten carbide beamstop is used to block the direct transmitted beam to prevent damage to the detector. **c**, Reconstruction of the initial magnetic domain state from a low-fluence-accumulated spectro-hologram with 58% circularly polarized x-ray pulses ($<$2 mJ/cm^2). The dark and light regions are 100-150 nm wide domains with opposite out-of-plane magnetization directions.

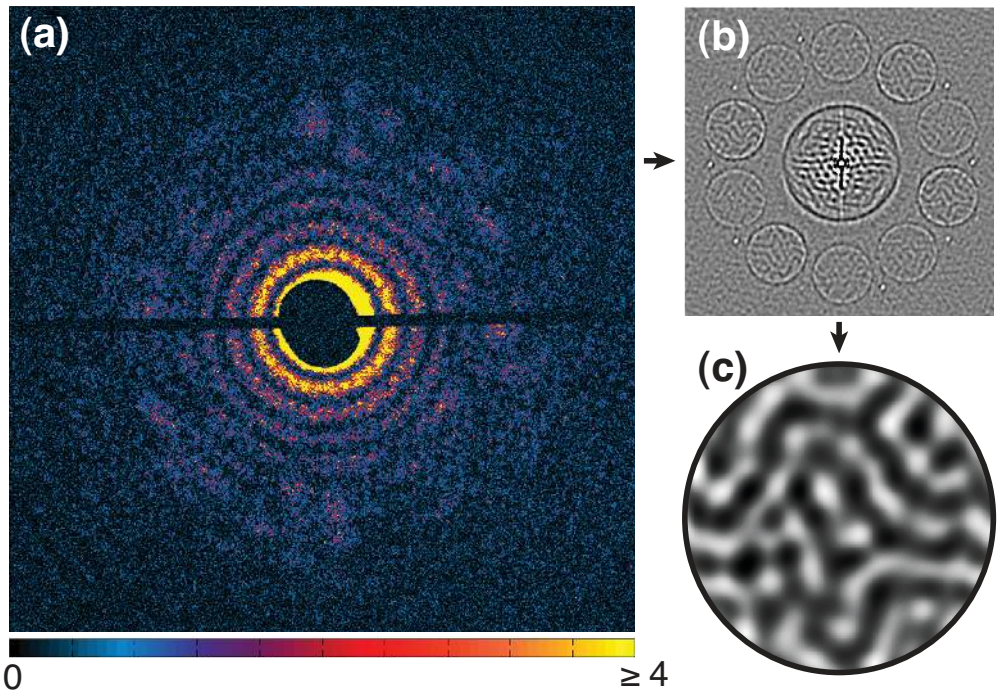

FIG. 2. Single-shot reconstruction of the nanoscale ferromagnetic ordering. **a**, X-ray spectrohologram from a 5-reference sample containing 1.5×10^5 detected photons from a 80 fs pulse. The scale bar unit is photon count per pixel. The corners shown here correspond to a momentum transfer of $0.054\,\mathrm{nm}^{-1}$. **b**, Real space magnitude of the complex autocorrelation after Fourier inversion of **a**. The center of the image is dominated by the self-correlation of the object and references. The complex conjugate pairs of object-reference cross-correlations are separated due to the off-axis geometry of the references, and the smaller, bright spots are the cross-correlation pairs between references. **c**, The final averaged reconstruction from **b** with a 10-90% resolution of 80 nm, which is limited by the reference size.

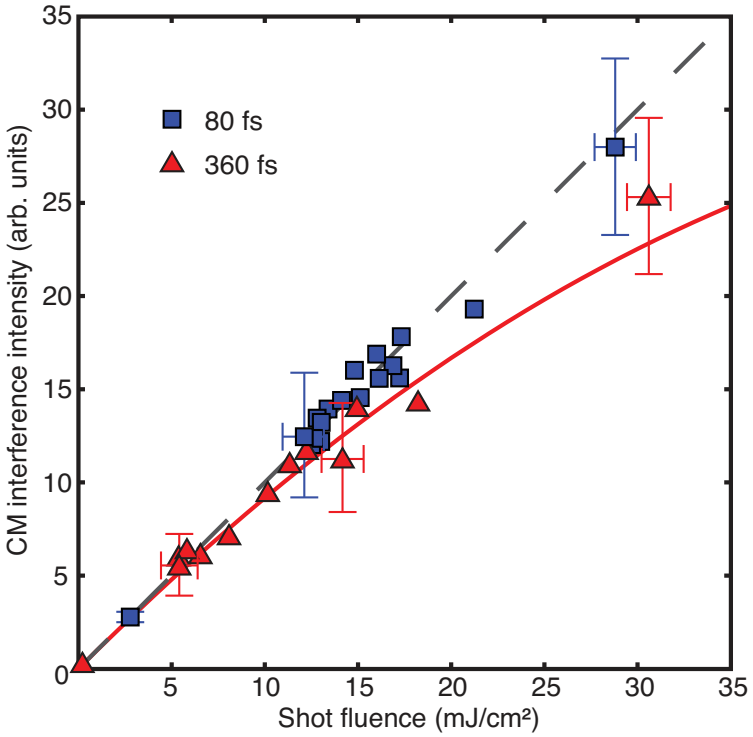

FIG. 3. Fluence dependence of charge-magnetic interference intensity for 80 and 360 fs single-shots. The errors are shot noise dependent and the bars shown are representative of other data points with similar fluences and photon statistics. For 80 fs pulses, the CMI intensity remains proportional to the incident x-ray fluence. This relation holds for low fluence 360 fs pulses, while a reduction of CMI intensity was observed at higher fluences indicating that x-ray-induced demagnetization occurred during the longer pulse durations. The reduction of CMI intensity is in agreement with calculations (red line) based on optically-induced ultrafast demagnetization with comparable amounts of energy deposited.

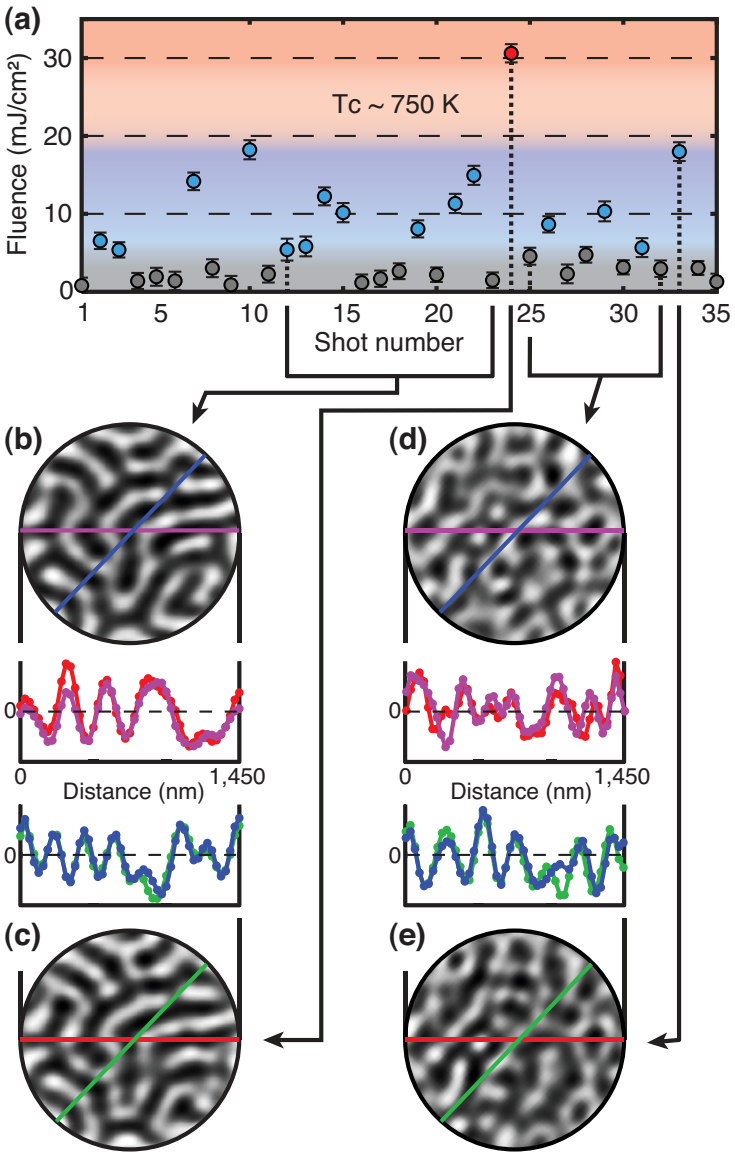

FIG. 4. Fluence thresholds and image correlations in single-shot images with 360 fs pulses. **a**, Fluence plot of the single-shot series. The blue markers represent pulses that are above the statistical threshold of 5 mJ/cm^2 for spectro-holographic imaging. The red marker represents the pulse with sufficient fluence to induce irreversible changes in the sample. Gray markers indicate pulses that are below the imaging threshold. Error bars indicate uncertainty due to shot noise. **b-c**, Average reconstruction from shots 12 to 23 and reconstruction from shot 24. **d-e**, Average reconstruction from shots 25 to 31 and reconstruction from shot 33. Line cuts show good agreement of the domain patterns shot-to-shot.